Adsorption of Phenol from Wastewater Using Calcined Magnesium-Zinc-Aluminium Layered Double Hydroxide Clay

Lehlogonolo Tabana, Shepherd Tichapondwa *, Frederick Labuschagne[ID] and Evans Chirwa[ID]

Department of Chemical Engineering, University of Pretoria, Lynnwood Rd, Hatfield, Pretoria 0002, South Africa; tabanashane@gmail.com (L.T.); johan.labuschagne@up.ac.za (F.L.); evans.chirwa@up.ac.za (E.C.)
* Correspondence: shepherd.tichapondwa@up.ac.za

check for
updates

Abstract: The presence of priority and emerging aromatic-based pollutants in water sources is of growing concern as they are not bioavailable and are present in reuse plant feed streams. These pollutants have known mutagenic and carcinogenic effects and must therefore be removed. Adsorption has been widely accepted as a suitable remediation technology due to its simplicity. Clay-based adsorbents have attracted significant attention due to their low cost, environmentally benign properties and regeneration potential. The present work focused on the thermal modification of a commercial Layered Double Hydroxide (LDH) clay and its subsequent effectiveness as an adsorbent in the removal of phenol from wastewater. Calcination of the neat clay resulted in the formation of metal oxides with varying phases and crystallinity depending on the treatment temperature. The BET surface area increased by 233% upon calcination at 500 °C. The highest phenol removal (85%) was observed in the clay calcined at 500 °C compared to 10% for the neat clay. Optimization studies revealed a maximum adsorption capacity of 12 mg/g at an adsorbent loading of 10 g/L at pH 7. Phenol adsorption was postulated to occur via a two-stage intercalation and surface adsorption mechanism. The equilibrium data were best fitted on the Freundlich isotherm model which describes heterogeneous adsorption. The adsorption kinetics followed a pseudo-second-order kinetic model with rate constants of 4.4×10^{-3} g/mg·h for the first 12 h and 6.1×10^{-3} g/mg·h thereafter.

Keywords: water treatment; hydrotalcite like; adsorption capacity; adsorption model

1. Introduction

Fresh water scarcity has become a major global challenge as many resources have been exhausted while others are being polluted due to rapid industrialization and increasing demand [1]. Emerging non-biodegradable organic pollutants are also becoming more prevalent in the effluent of wastewater treatment plants due to the inadequacy of conventional wastewater treatment processes. Phenol and its derivatives are some of the recalcitrant organic pollutants which are prevalent in waterbodies and emanate from domestic waste, industrial effluents, municipal landfill leachates, as well as agricultural runoffs. Phenolic compounds have been found to be mutagenic and carcinogenic and may result in serious health risks for humans, animals, and aquatic life if left untreated [2]. The World Health Organization (WHO) stipulates that the maximum permissible limit for phenol in drinking water is 2 ppm [3]. Water reuse has been touted as one of the most promising alternative sources of drinking water, with several plants already in operation across the world [4,5]. The efficiency of this technology depends on its ability to remove the intractable organic pollutants that remain untreated in the effluent of conventional biological wastewater treatment plants [6]. Various physical,

biological, chemical and electrochemical treatment technologies have been used for the removal of such pollutants from water [7]. Adsorption-based processes have widely been used due to their low operational cost, simplicity, high efficiency, ease of handling, low energy demand, minimal sludge generation and the possibility of regeneration [8,9]. Activated carbon is the most widely used adsorbent for the removal of refractory compounds due to its high surface area and hydrophobic surface. However, the production and regeneration costs of activated carbon have limited its application in wastewater remediation. This has led to the prospect of using alternative low-cost adsorbents such as clays for wastewater remediation. Clay minerals can be divided into three categories according to their ion exchange property, namely nonionic, cationic and anionic clays [10]. All three categories have been found to be good adsorbents for various impurities in wastewater. For example, Cavallaro, Lazzara, Rozhina, et al. [11] reported that halloysite, a nonionic clay, efficiently removed dyes from aqueous solutions, while vermiculite, a cationic clay, was able to remove chromium from tannery effluent [12]. The present study focused on the use of anionic LDH clays and their potential.

LDH clays have been shown to possess properties which are favorable for adsorption of several pollutants in aqueous solutions [13]. They are classified as anionic clays which consist of brucite-like hydroxide sheets where partial substitution of trivalent with divalent cations results in a net positive charge in the sheets which is counter balanced by anions within interlayer spaces [14]. In nature, these clays can be found as minerals which result from the precipitation of basalts in saline water [15]. LDH clays can also be synthesized through relatively low-cost processes such as co-precipitation, regeneration, hydrothermal crystallization urea hydrolysis and sol-gel methods [16]. Labuschagne, Wiid, Venter, et al. [17] developed a green, zero effluent synthesis method which produces LDH in an economic and environmentally friendly manner. LDH clays can remove impurities from aqueous solutions through several mechanisms, such as surface adsorption, intercalation, adsolubilization of organics with organo-modified LDH [18] and reconstruction of calcined clays. Numerous authors have investigated the use of LDH clays as adsorbents for the removal of various impurities in aqueous solutions such as dyes [19,20], heavy metal cations [21,22] and phenolic compounds [23]. Some of the main LDH properties that give rise to good adsorption properties include surface area, crystallinity, composition and surface chemistry [24]. Chen, Y., Chen, H.-R. and Shi [25] reported that a higher adsorption capacity ca. 760 mg/g of LDH of diclofenac using LDH was mainly due to the large surface area of the clay. Zaghouane-Boudiaf, Boutahala and Arab [19] reported that calcination of a Magnesium-Nickel-Aluminium LDH resulted in the formation of amorphous metal oxides which had a higher methyl orange adsorption capacity than the neat clay.

While the removal of dyes and other impurities, such as acidity of metal cations, have been thoroughly articulated in literature, the removal of phenol and other non-polar compounds using calcined LDH clays has not been well-investigated to the best of our knowledge. The current study aims to evaluate the effectiveness of remediating phenol from wastewater using calcined commercial Magnesium-Zinc-Aluminum LDH clay.

2. Materials and Methods

2.1. Materials

Magnesium-Zinc-Aluminum Carbonate (Mg-Zn-Al (CO_3)) hydrate clay, referred to as neat clay, was obtained from Clariant, Germany. Phenol used to prepare the simulated phenolic wastewater was obtained from Merck, South Africa. Analytical grade acetonitrile and acetic acid which were used as mobile phase in High Performance Liquid Chromatography (HPLC) were procured from Sigma Aldrich. The sodium hydroxide used for pH adjustment was also procured from Sigma Aldrich, South Africa. Deionized water was used for all dilutions and standards preparations.

2.2. Adsorption Experiments

2.2.1. Calcination

Calcination of the clay was carried out in an Aluminium Electric Muffle Furnace at 250, 500 and 1100 °C, respectively. Neat clay samples weighing ca. 50 g were placed in porcelain crucibles and covered with a lid before charging them into the furnace at the pre-set temperature for 4 h. The resultant product was collected for further tests and analysis upon cooling. The residues obtained from the neat clay calcined at 500 °C are referred to as calcined clay in the subsequent sections of this work.

2.2.2. Adsorption

The first set of tests compared the adsorption efficiency of the heat-treated clays to that of the neat clay. In these tests, 100 mL of simulated wastewater containing 40 mg/L phenol was contacted with 10 g/L of clay in a 250 mL glass beaker. The resulting suspension was stirred continuously for 24 h to allow for maximum adsorption. The suspension was then centrifuged at 9000 rpm for 10 min, the centrate was further refined by filtering through a 0.45 μm Millipore filter. The solids remaining from the centrifuging process were left to dry in open air, after which they were milled and taken for further analysis. Once the best performing clay was identified, it was used for further optimization studies. The optimum clay loading was determined by adding clay loadings of 5, 10, 15, and 20 g/L to 40 mg/L phenol solutions and contacting for 24 h. Phenol adsorption using LDH clay was found to reach equilibrium within 24 h [24], hence it was the longest residence time for this study. The effect of pollutant concentration was determined by varying the phenol concentrations as follows: 20, 40, 80, 120 and 200 mg/L while maintaining an adsorbent loading of 10 g/L. The influence of solution pH was investigated at values of 7, 9 and 12. A 1 M sodium hydroxide solution was used to adjust the pH. It should be noted that no experiments were conducted in the acidic pH range since it is known to damage the structure of the LDH clay [14,26,27]. Once the optimum conditions were determined, adsorption tests were carried out under these conditions and samples were taken on an hourly basis for the first two hours, and every two hours thereafter for 24 h in order to investigate the kinetics. The solids collected after contacting the phenolic water for 24 h are referred to as spent clay in the results section of this work. All the solution samples obtained from the above-mentioned experiments were analyzed using a Waters Alliance 2695 Separations HPLC Module equipped with an auto sampling unit and a Photodiode Array Detector (PDA). Separations were performed on a C18 waters column using isocratic elution with 70% acetonitrile solution (99% (v/v) acetonitrile and 1% acetic acid) and 30% water (99% deionized water and 1% acetic acid) at a flowrate of 1 mL/min. The adsorption efficiency in terms of percentage of phenol (R) and the equilibrium amount of phenol adsorbed (q_e) were determined as shown in Equations (1) and (2), respectively. Where C_o, C_t and C_e (mg/L) represent the initial phenol concentration, concentration at time = t and equilibrium concentration, respectively; V (L) is the volume of the solution, while m (g) represents the mass of adsorbent used, q_e (mg/g) is the adsorption amount on clay at equilibrium.

$$R = \left(1 - \frac{C_t}{C_0}\right) \times 100\% \tag{1}$$

$$q_e = \frac{V}{m}(C_o - C_e) \tag{2}$$

2.3. Characterization

The compositions and phases of the neat and calcined clays were analyzed using a PANalytical X'Pert Pro powder diffractometer in θ–θ configuration with an X'Celerator detector and variable divergence and fixed receiving slits with Fe-filtered Co-Kα radiation (λ = 1.789 Å). Samples were prepared according to the standardized Panalytical backloading system which provides for near-random

distribution of the particles. Data was collected in the angular range 5 to 90° 2θ with a step size of 0.008° 2θ and 13 s scan step time. The mineralogy was determined by selecting the best–fitting pattern from the Inorganic Crystal Structure Database (ICSD) to the measured diffraction pattern, using X'Pert Highscore Plus software. The elemental composition of the clay samples was determined by x-ray fluorescense (XRF) analysis. A Thermo Fisher ARL Perform'X Sequential XRF instrument with Uniquant software was used to collect the data. The loss on ignition was determined by roasting the sample (placed in alumina refractory crucible) at 1000 °C. The average particle size and morphology of the clays were analysed using scanning electron microscopy (SEM). The images were obtained using a Zeiss Ultra Plus scanning electron microscope. SEM samples were prepared by distributing the samples on carbon tape stuck to a microscopy stub; the samples were then sputter coated with carbon under argon gas. The thermal phase transitions of the clay samples were tracked by weighing out 5.2, 4.5 and 4.8 mg of neat, spent and calcined clay into alumina crucibles before running the sample on a TA instrument, Q5000 thermogravimetric analyzer (TGA). All the samples were subjected to a temperature scan from 25 to 950 °C at a heating rate of 10 °C/min in nitrogen atmosphere. The Brunauer Emmett Teller (BET) surface areas were determined using a Micrometrics Tristar 3000 BET analyser. All samples were degassed for 24 h at 150 °C under a 10^{-5} Torr vacuum before analysis.

3. Results

3.1. Characterization

X- Ray Fluorescence (XRF) analysis showed that the neat clay contained ca. 16, 23 and 19% (*w/w*) aluminium, magnesium and zinc, respectively, with a loss on ignition of 42%. The corresponding molar composition was determined to be 0.676 for the divalent metals and 0.324 for the trivalent aluminium which is an almost perfect 2:1 divalent/trivalent ratio LDH. Based on these values, the chemical formula of the neat clay was postulated to be: $Mg_{3.27}Zn_{1.01}Al_2(OH)_{12.83}CO_3 \cdot nH_2O$. The compositions of $CO_3{}^{2-}$ and OH^- were calculated with the theoretical equations using the experimentally obtained metallic ratios. This correlates exceptionally well with the general chemical formula for hydrotalcite-like materials, $Mg_xZn_yAl_2(OH)_{2(2+x+y)}CO_3 \cdot nH_2O$ where x and y are less than 4 while n is less than 10 [28].

3.1.1. Thermal Analysis

The thermogravimetric analyses of the neat, calcined and spent clay are shown in Figure 1. A two-stage thermal decomposition of LDH clay is widely reported; at low temperatures (up to 225 °C) interlayer water was desorbed, while the decomposition of interlayer carbonate and dehydroxylation of metal hydroxide occurred at higher temperatures (225–500 °C) [29]. Zhao, Li, Zhang, et al. [30] reported that decomposition at higher temperatures can occur in two distinct steps when the Mg^{2+}/Al^{3+} ratio is equal to two. The first of these two steps was attributed to the partial loss of OH^- from hydroxide layers while the second step was due to the complete loss of OH^- and carbonate anions [31]. In the present study, the neat clay exhibits thermal decomposition in three stages which resembles the behavior reported in literature for LDH having a divalent/trivalent ratio of 2, as shown in Figure 1a,b. The maximum loss of interlayer water occurred at 190 °C (13%), followed by what is envisaged to be partial loss of OH^- from hydroxide layers at 250 °C (6%) until the complete dehydroxylation and decomposition of carbonate occurred at 410 °C. The latter step showed a wide peak indicating a slow process and had mass loss of ca. 21%. The maximum loss of interlayer water in the spent clay occurred at 100 °C (9%), while dehydroxylation, decomposition of carbonate and any adsorbed phenol occurred at 345 °C (16%), as shown in Figure 1a,d. The shift in decomposition stages of spent clay to lower temperatures can be attributed to the reduced strength of hydrogen bonding which is known to keep water molecules in close interaction with interlayer carbonate anions and hydroxide layers [29]. The maximum weight loss for spent clay was low at 25% compared to 40% of neat clay because the spent clay contained an appreciable amount of the stable spinel ($MgAl_2O_4$) phase. No appreciable mass loss was displayed by the clay calcined at 500 °C and above, since its structure had already been

converted to metal oxides, as displayed in Figure 1a,c. Any further increases in temperature were likely to alter the crystal phase of the metal oxides. Milanovic [32] reported that the residues of a complete dehydroxylation and decomposition of interlayer carbonate anions were mainly periclase (MgO) and spinel ($MgAl_2O_4$) phases.
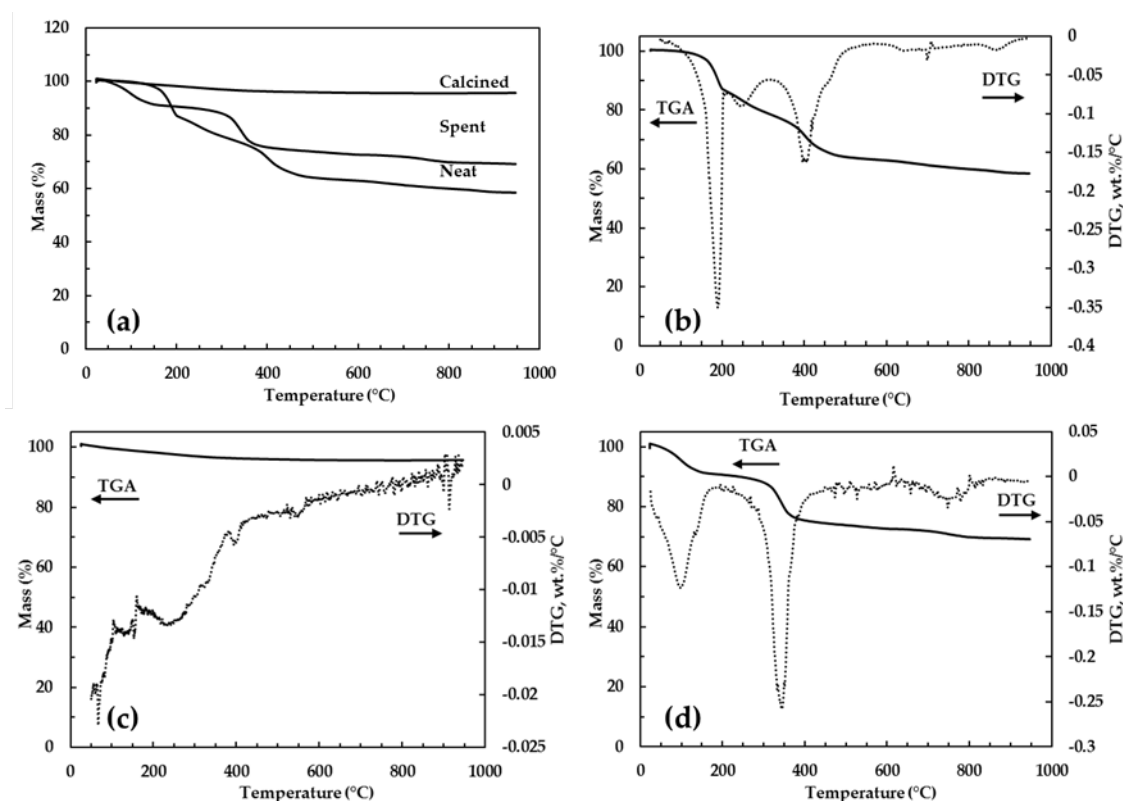

Figure 1. TGA curves of the neat, calcined and spent clay (**a**); TGA and DTG curves of the neat clay (**b**), calcined clay (**c**) and spent clay (**d**).

3.1.2. X-ray Diffraction (XRD) Spectra

Figure 2 shows the XRD spectra of the clays treated at various calcination temperatures. The clay calcined at 250 °C maintained a similar structure to the neat clay even though it showed signs of reduced crystallinity. A significant change was, however, noticed in the (003) plane; this was attributed to a partial loss of interlayer molecules signaling the onset of the metal oxide formation [32,33]. The XRD spectra for clays calcined at 500 and 1100 °C showed periclase (MgO) and spinel ($MgAl_2O_4$) as the dominant phases present. LDH clay calcined at 500 °C resulted in more amorphous products and featured periclase and spinel with a distribution of 59% and 41%, respectively. The sharp peaks obtained after calcination at 1100 °C signaled the presence of highly crystalline oxides which were identified as 39% periclase and 61% spinel. This corresponds with suggestions from the literature that calcination above 850 °C leads to a significant increase in the spinel content and highly crystalline residues [32,33].

3.1.3. Brunauer Emmett Teller Surface Area

The BET surface area of clay calcined at 500 °C (30 m^2/g) was 3 times higher than that of the neat clay (9 m^2/g). The increase in surface area upon calcination is attributed to a combination of phase changes from LDH to mixed oxides as a result of temperature treatments together with the development of pores and channels which are formed when water and carbon dioxide are driven out of the clay interlayers [32]. The clay calcined at 250 °C showed a slight increase in BET surface area

to 12 m^2/g compared to the neat clay. This can be attributed to the partial breakdown of the LDH structure. There was a decrease in BET surface area on the clay calcined at 1100 to 19 m^2/g compared to the clay calcined at 500 °C as highly crystalline phases were formed.
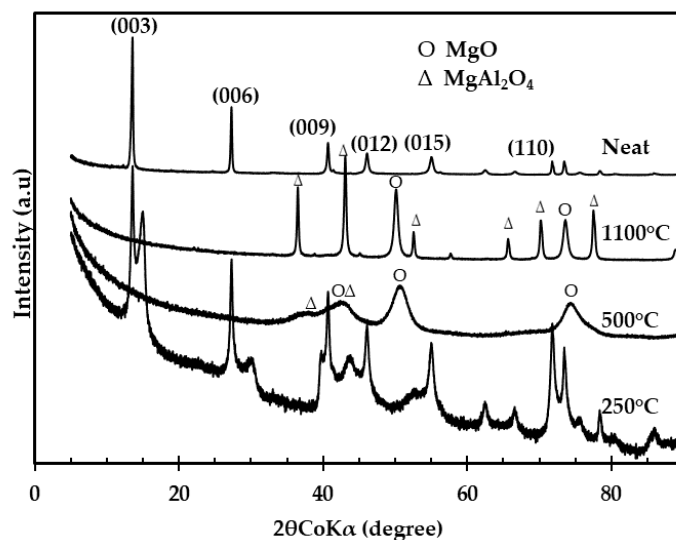

Figure 2. X-ray diffraction spectra of clay calcined at various temperatures.

3.1.4. Scanning Electron Microscopy

Figure 3 shows the morphology of the neat, calcined, spent clay and recalcined clay. The neat clay (Figure 3a) featured hexagonal plate-like particles. This observation was consistent results from other researchers who reported on magnesium and aluminium based LDH clays [34]. Upon calcination, the ordered hexagonal platelets were destroyed, and irregular mixed metal oxide particles were formed (Figure 3b). Figure 3c depicts the morphology of the particles obtained after contacting the calcined clay with the simulated phenol wastewater. Though slightly more agglomerated, these particles had a similar platelet-like morphology to that observed in Figure 3a. This observation confirms the ability of LDH clays to reconstruct from their calcination products once in contact with water. One of the key requirements for a practical adsorbent is its ability to be regenerated; Figure 3d shows the particle morphology obtained following the recalcination of the pollutant.
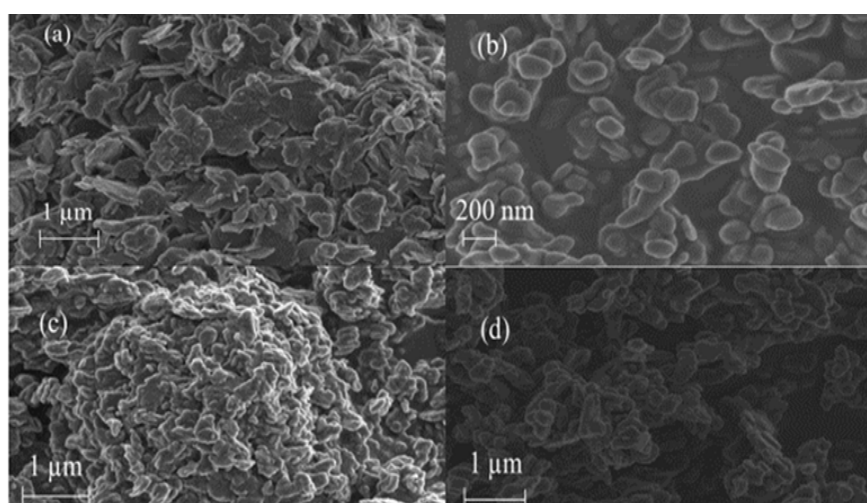

Figure 3. SEM images of the neat (**a**), calcined (**b**), spent (**c**) and recalcined clay(**d**).

3.2. Adsorption Results

3.2.1. Effect of Calcination Temperature

Figure 4 shows phenol adsorption efficiencies of the neat and calcined clay at various temperatures. Both the neat and 250 °C-calcined clay attained phenol removals below 10%; this was expected since the structure and composition of the two clays were virtually similar despite the thermal treatment. Higher phenol adsorption efficiencies of 85% and 50% were observed for clay calcined at 500 and 1100 °C, respectively. These higher phenol removal values were ascribed to the presence of the amorphous periclase (MgO) phase. This accession is in line with results from other researchers who found excellent organic pollutant removal rates using amorphous nanosized metal oxides such as MgO, CaO, Al_2O_3 and MnO_2 as adsorbents [35–37]. The decrease in adsorption efficiency of ca. 37% when calcination temperature was increased from 500 to 1100 °C was postulated to be a result of an increase in the crystallinity and spinel content of the calcination products. It should also be noted that the higher adsorption observed for clays calcined at 500 °C and above can also be due to phenol being incorporated into the interlayer galleries of the LDH during reconstruction. Since the LDH clay calcined at 500 °C had the highest phenol removal, it was used as the primary adsorbent in all subsequent experiments.
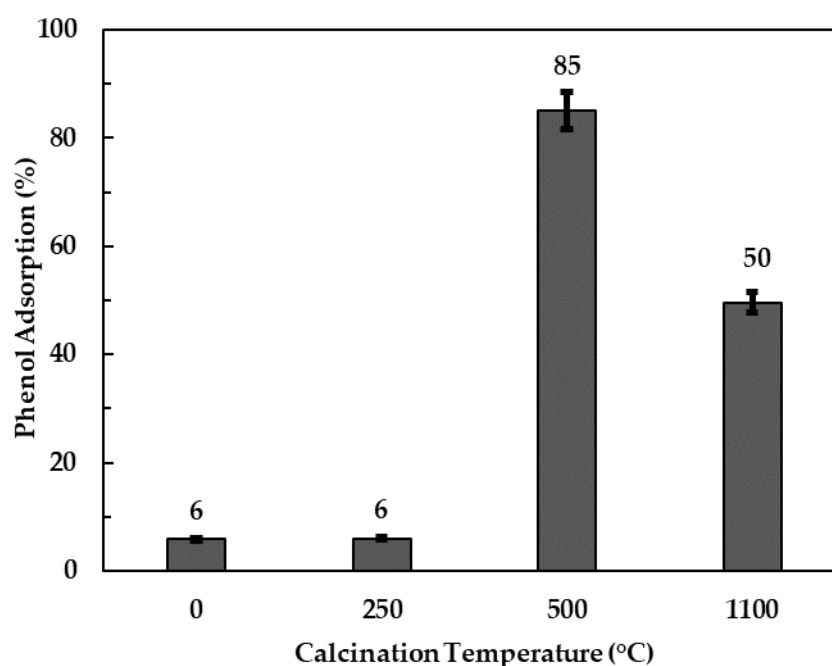

Figure 4. Adsorption efficiency of the clay calcined at various temperatures.

3.2.2. Effect of Adsorbent Loading

Figure 5 shows the phenol adsorption efficiencies as a function of adsorbent loading. A 15% increase in phenol adsorption was observed when the clay loading increased from 5 g/L (68%) to 10 g/L (83%). Marginal increases in phenol adsorption efficiencies (3% and 5%) were observed when clay loadings were further increased to 15 and 20 g/L. An increase in adsorbent loading is generally expected to increase the adsorption efficiency due to an increase in adsorption sites. According to Zubair, Daud, McKay, et al. [13] the dispersion of an adsorbent in aqueous solution is uniform below a certain limit at which all the active sites are fully exposed and accessible by adsorbates. The surfaces of most solid adsorbents are heterogeneous and are characterized by varying adsorption energies [38]. During adsorption, the sites are taken up sequentially, starting from the highest-energy sites to the lowest-energy sites. An increase in adsorbent loading beyond the optimum limit can result in

decreased dispersion efficiency leading to agglomerate formation and blocking of adsorption sites. It is hypothesized that a similar phenomenon might have taken place in the current study, leading to the marginal increase in phenol removal beyond 10 g/L loading.
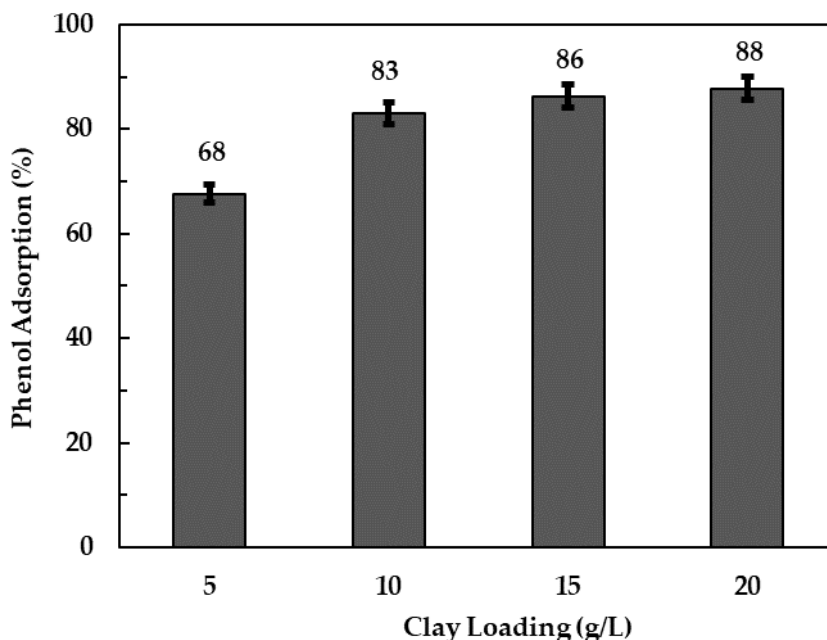

Figure 5. Phenol adsorption efficiencies at various clay loadings of 500 °C-calcined LDH.

3.2.3. Effect of pH

The initial pH of contaminated water is an important parameter for the efficient removal of pollutants using LDH clays. LDH clays can neutralize hydrogen ions in solution with low pH, while they get deprotonated in solutions with high pH [39]. In this study, the effect of initial pH on the adsorption of phenol was evaluated over the 7–12 pH range, with pH 7 indicating simulated wastewater with no pH adjustment. The results shown in Figure 6 indicate a low adsorption rate at high pH. This can be attributed to an increase in hydroxyl ions at higher pH values, thereby increasing the LDH reconstruction rate. Since the hydroxyl ions have high affinity for LDH compared to phenol, an increase in hydroxyl ions will lead to a decrease in intercalation of phenolate ions. These observations are similar to those presented by Zaghouane-Boudiaf, Boutahala and Arab [19] who reported that the removal of methyl orange in aqueous solution by LDH decreased as OH^- increased. Gong, Li, Wang, et al. [26], Dos Santos, Gonçalves, Constantino, et al. [14] and Zhang, Gong, Liu, et al. [40] reported that the adsorption of dyes from acidic aqueous solutions using calcined LDH was less compared to the adsorption from neutral solution due to the dissolution of LDH at lower pH. Based on this background, acidic conditions were not considered for this work. It should be noted that measurements of the equilibrium pH after 24 h contact time did not reveal a marked difference from the initial pH. The removal of phenol with calcined LDH clay was therefore optimum at neutral pH of polluted water and the proceeding adsorption equilibrium tests were conducted at this pH.
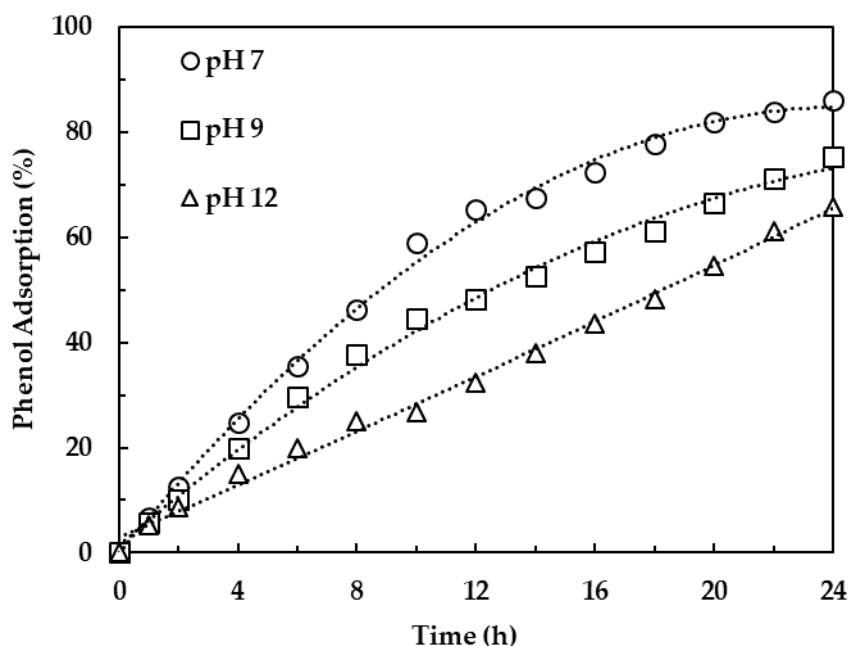
Figure 6. Effect of pH on phenol adsorption.

3.2.4. Adsorption Isotherms

In order to gain some insights into the nature of interaction between the calcined LDH clay and the phenol solution, experimental adsorption data was fit to the widely used Langmuir and Freundlich isotherm models [7]. These models are represented by the terms in Equations (3) and (4), respectively.

$$q_e = \frac{Q_L K_L C_e}{1 + K_L C_e} \tag{3}$$

$$q_e = K_f C_e^{\frac{1}{n}} \tag{4}$$

Where, Q_L (mg/L) and K_L (L/mg) are Langmuir constants related to the loading energy and adsorption, K_f (mg/g), (L/mg)$^{1/n}$ and n are Freundlich constants.

The Langmuir isotherm was developed with an assumption that homogeneous adsorption occurs on the adsorbent with all sites possessing uniform energy [41]. According to Dada, Olalekan, Olatunya, et al. [42], the Langmuir isotherm is valid for monolayer adsorption onto a surface containing a finite number of identical sites. The Freundlich adsorption isotherm is mostly applied to heterogeneous adsorption and chemisorption processes [43]. Sepehr, Al-Musawi, Ghahramani, et al. [44] described the Freundlich equilibrium isotherm as an empirical equation used for the description of multilayer adsorption with interaction between adsorbed molecules. Equilibrium concentrations obtained at various initial concentrations were used to plot the adsorption isotherm profiles; whereby the equilibrium amount (q_e, mg/g) was plotted as a function of the equilibrium concentration in the solution (C_e, mgL). The non-linear form of both models was used in order to avoid changing the error structure of the experimental data during the transformation of adsorption isotherms to their linearized forms [45]. Figure 7 and Table 1 show the adsorption data and adsorption isotherms parameters, respectively. The equilibrium data was found to fit the Freundlich model better as it gave a correlation coefficient (R^2) of 0.998 as compared to 0.969 for the Langmuir isotherm. This indicates that the phenol adsorption onto LDH clay is a heterogeneous process. The heterogeneity factor was determined to be above unity and less than 10 at 2.2, indicating a physical adsorption process. The maximum adsorption capacity was estimated to be 12 mg/g through the Langmuir isotherm.
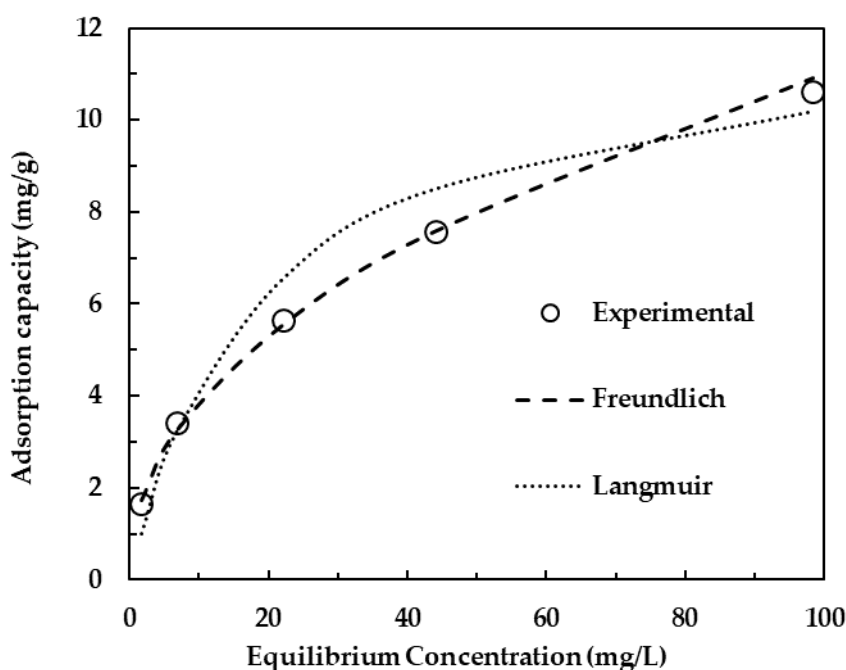
Figure 7. Phenol adsorption isotherms.

Table 1. Adsorption isotherm parameters.

	Adsorption Isotherm	
Parameter	Freundlich	Langmuir
K_L	-	0.053
Q_L	-	12.1
K_F	1.36	-
n	2.21	-
R^2	0.998	0.969

3.2.5. Adsorption Mechanism

Figure 8 shows the XRD spectra of the neat and the calcined clay before and after adsorption (at various residence times). The neat clay shows sharp diffraction peaks at low 2θ values with planes of (003) and (006) and small diffraction peaks at higher 2θ values, which can be expected from LDH clays [46]. The presence of mixed-metal oxides from the calcined clay was apparent through their respective diffraction peaks: MgO (2θ = 52° and 70°) and $MgAl_2O_4$ (2θ = 37° and 43°). The diffraction peaks after adsorption at the plane (003) shifted to the lower 2θ values; this was attributed to an increase in d-spacing due to adsorbed phenol. The d-spacing after adsorption as determined by Bragg's law was 8.25 Å having increased from a d-spacing of 7.57 Å (for neat clay). It was further observed that the clay fully reconstructed after 12 h, however, phenol adsorption efficiency at that time was ca. 65%, as displayed in Figure 6. There was no further increase in d-spacing after 12 h even though more phenol was removed from wastewater. This showed that no further intercalation occurred after 12 h. Therefore, it can be concluded that a dual process mechanism exists for phenol adsorption using calcined clay. Both intercalation and adsorption occur in the early stages until the clay is fully reconstructed; thereafter, surface adsorption becomes the dominant process. Chen, H., Hu, Chen, M., et al. [23] reported that the degree of phenolate adsorption by intercalation into a calcined Mg-Al-CO₃—LDH was about 3.6%, with most of phenolate ions adsorbed on the surface. This showed that phenol removal from aqueous solutions with LDH clay is achieved through a two-stage process mechanism. They concluded that less phenolate was intercalated because the bulky hydrophobic phenyl ring in phenolate was unable to provide electrostatic interaction with the hydroxide layer, thereby showing weaker affinity

for LDH clay. Figure 8 further shows the disappearance of the diffraction peaks associated with the periclase phase while the spinel phase at 2θ = 37° and 43° remained unchanged as the clay underwent a reconstruction process. Two more diffraction peaks associated with the spinel phase became clearer at 2θ = 70° and 78°. This confirmed the lack of adsorption activity by the spinel phase. The XRD spectra from the residues obtained after 24 h indicated the reduction in crystallinity as the peaks associated with hydrotalcite were not as sharp and prominent as the neat clay.
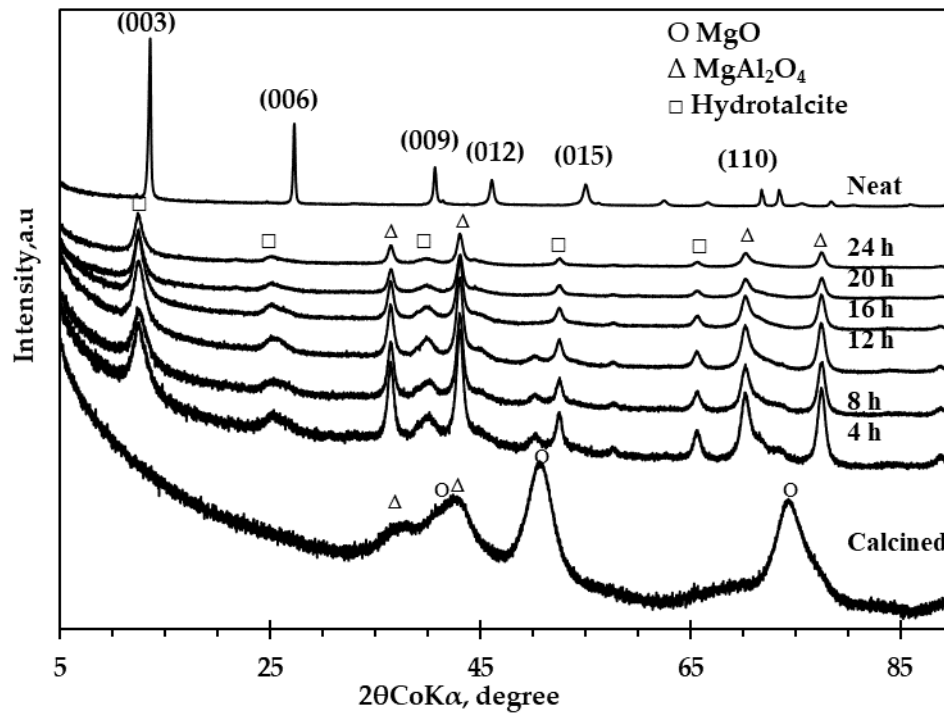

Figure 8. X-ray diffraction spectra of the neat, calcined and spent clay at various residence times.

3.2.6. Adsorption Kinetics

Modelling of the adsorption rate and the establishment of time dependence under various process conditions helps with practical applications of adsorption such as process design and control. The kinetics of a process details how fast the rate of chemical reaction occurs and the factors affecting it. The two frequently used kinetics models for adsorption processes are the pseudo-first-order and the pseudo-second-order models. The linearized equations for the pseudo-first-order and pseudo-second-order models shown by Equations (5) and (6), respectively. Chingombe, Saha and Wakeman [47] reported that sorption reactions can be represented by three mechanisms, namely: (1) film or surface diffusion where sorbate is transported from the bulk solution to the external surface of the sorbent; (2) intraparticle or diffusion, where sorbate molecules move into the interior of the sorbent particles and (3) sorption on the interior sites of the sorbent.

$$\log(q_e - q_t) = \log q_e - \frac{k_1}{2.303}t \tag{5}$$

$$\frac{1}{q_t} = \frac{1}{k_2 q_e^2}\left(\frac{1}{t}\right) + \frac{1}{q_e} \tag{6}$$

where k_1 (h^{-1}) and k_2 (g/mg·h) represent the pseudo-first-order and pseudo-second-order rate constants respectively; q_e (mg/g) and q_t (mg/g) represent the amount of phenol adsorbed at equilibrium and time t (h), respectively.

In the present study, surface or film diffusion can be ignored since vigorous, turbulent mixing was maintained throughout the experiments. Therefore, a two-stage adsorption mechanism as detailed in Section 3.2.5 was proposed. Phenol adsorption kinetics fit the pseudo-second-order model as shown in Figure 9, with the time interval divided between 0 to 12 h (Figure 9a) and 14 to 24 h (Figure 9b). This result is in line with the study done by Simonin [48] who reported that the pseudo-first-order and the pseudo-second-order models were controlled by diffusion and adsorption reaction at the liquid/solid interface in the adsorbent, respectively. The equilibrium adsorption amount (q_e), k_2 (between 0 and 12 h) and k_2 (between 14 and 24 h) were determined to be 8.05 mg/g, 4.41×10^{-3} g/mg·h and 6.05×10^{-3} g/mg·h, respectively. The phenol removal rate was slower for the first 12 h as the phenolate ion competed with both the carbonate ($CO_3{}^{2-}$) and hydroxyl (OH^-) for intercalation; since LDH clay has strong affinity for $CO_3{}^{2-}$ and OH^-, less phenolate was intercalated.
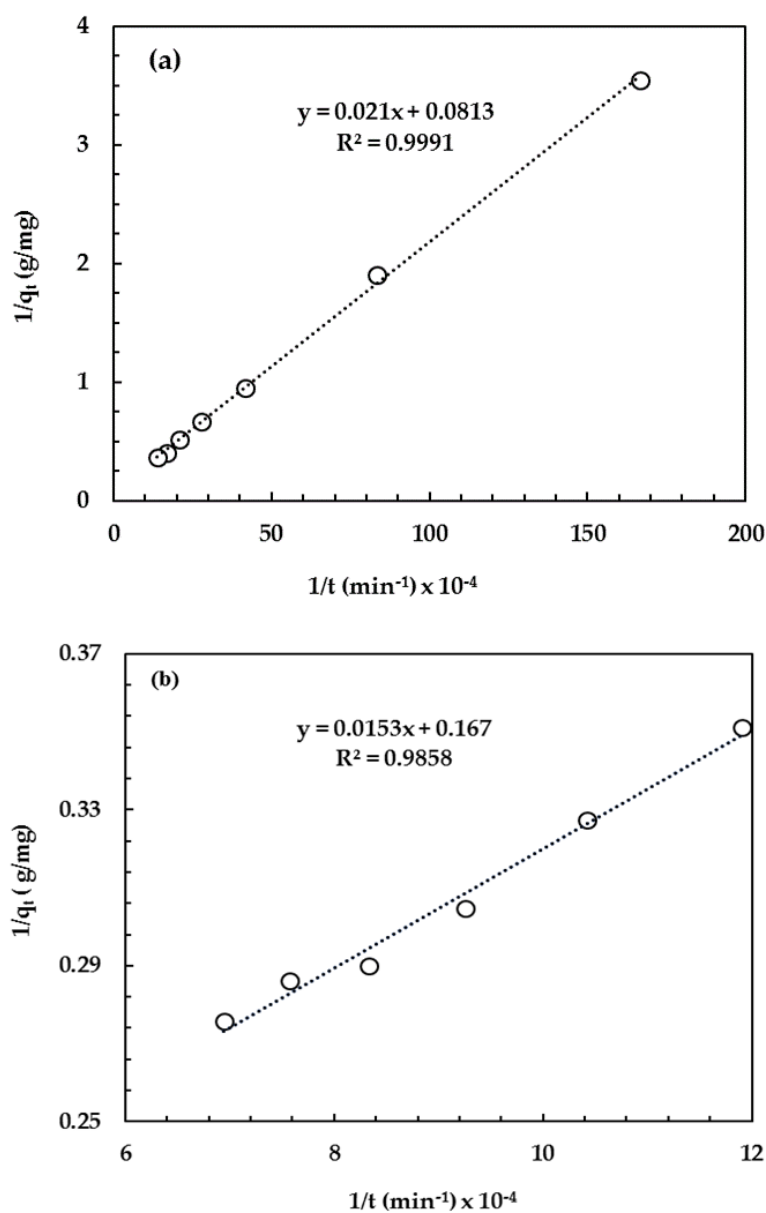

Figure 9. Phenol adsorption kinetics ((**a**) represents kinetic data up to 12 h; (**b**) represents kinetic data from 14 h to 24 h).

3.2.7. Clay Regeneration and Reusability

Recycling and reusability of an adsorbent is an important aspect for the viability of the adsorption process. Calcined LDH clays are capable of being regenerated due to a "memory effect". Phenol adsorbed on the LDH clay can be completely decomposed upon re-calcination of the spent clay, hence the suspensions were recovered after completing equilibrium adsorption experiments and recalcined at 500 °C for 4 h. The adsorption efficiencies of phenol using regenerated clay after thermal recycling are shown in Figure 10. The reduction in phenol adsorption over the first 3 cycles was relatively small at 2% (from 86 to 84%). There was a significant decrease in phenol adsorption efficiency of 25% on the fourth cycle. These results showed that thermal regeneration of clay for re-use is only feasible over three cycles after which the clay loses its sorption capacity. This was also observed by Zhang, Ni, Xia, et al. [49] when they investigated the removal of Naphthol Green B from aqueous solution by calcined LDH clay. Zhu, Li, Xie, et al. [50] reported that clay can lose its adsorption capacity upon repeated calcinations due to a decrease in its crystallinity. Alcaraz, Arena, Gillespie, et al. [51] reported that the spinel content increased upon calcination of clay above 850 °C or on repeated calcination steps which leads to a decrease in the clay's adsorption capacity.
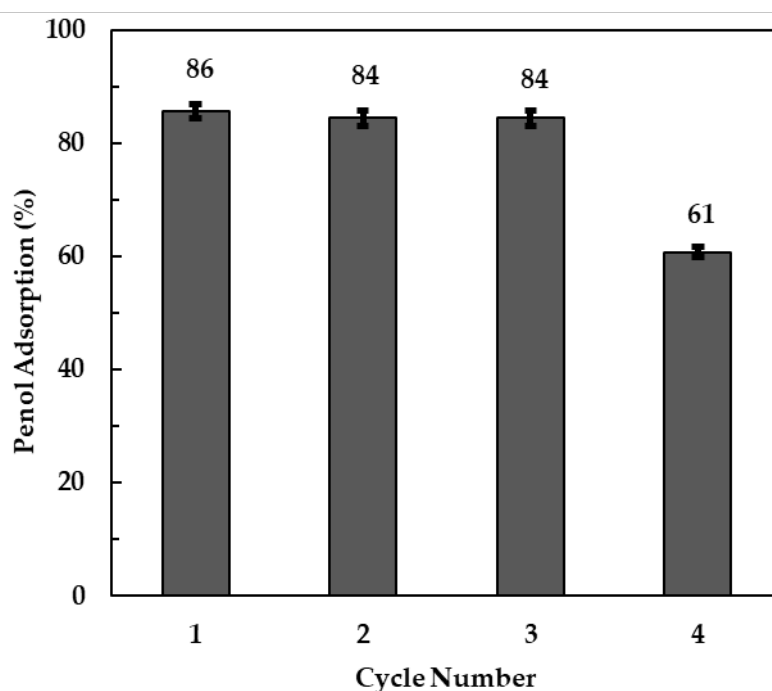

Figure 10. Phenol adsorption efficiencies on regenerated and re-used clay.

4. Conclusions

Calcination of commercial Magnesium-Zinc-Aluminium Carbonate LDH clay at 500 °C produced mixed metal oxides which served as good adsorbents for phenol as more than 85% phenol was adsorbed over 24 h. A clay loading of 10 g/L and neutral pH conditions were found to be the optimum conditions for phenol removal from wastewater. A two-stage phenol removal mechanism was hypothesized and comprised of intercalation and surface adsorption during the first 12 h, followed by surface adsorption up to 24 h. The reaction kinetics were best-described by the pseudo-second-order model while the adsorption equilibrium data indicated a heterogeneous distribution of the adsorbate since the Freundlich isotherm model showed the highest regression coefficient values.

Author Contributions: Conceptualization, S.T.; investigation, L.T.; methodology, L.T. and S.T.; writing: original draft preparation, L.T.; writing: review and editing, S.T. and F.L.; formal analysis, E.C.; funding acquisition, S.T. and F.L.; resources, E.C. All authors have read and agreed to the published version of the manuscript.

Conflicts of Interest: The authors declare no conflict of interest.

References

1. Kumar Reddy, D.; Lee, S. Water pollution and treatment technologies. *J. Environ. Anal. Toxicol.* **2012**, *2*, e103. [CrossRef]

2. Olujimi, O.; Fatoki, O.; Odendaal, J.; Okonkwo, J. Endocrine disrupting chemicals (phenol and phthalates) in the South African environment: A need for more monitoring. *Water SA* **2010**, *36*. [CrossRef]

3. World Health Organization. *Cresols: Health and Safety Guide*; WHO: Geneva, Switzerland, 1996.

4. Anderson, J. The environmental benefits of water recycling and reuse. *Water Sci. Technol. Water Supply* **2003**, *3*, 1–10. [CrossRef]

5. Dolnicar, S.; Hurlimann, A. Drinking water from alternative water sources: Differences in beliefs, social norms and factors of perceived behavioural control across eight Australian locations. *Water Sci. Technol.* **2009**, *60*, 1433–1444. [CrossRef]

6. Yasui, H.; Miyaji, Y. A novel approach to removing refractory organic compounds in drinking water. *Water Sci. Technol.* **1992**, *26*, 1503–1512. [CrossRef]

7. Alqadami, A.A.; Khan, M.A.; Otero, M.; Siddiqui, M.R.; Jeon, B.-H.; Batoo, K.M. A magnetic nanocomposite produced from camel bones for an efficient adsorption of toxic metals from water. *J. Clean. Prod.* **2018**, *178*, 293–304. [CrossRef]

8. Yin, N.; Wang, K.; Wang, L.; Li, Z. Amino-functionalized MOFs combining ceramic membrane ultrafiltration for Pb (II) removal. *Chem. Eng. J.* **2016**, *306*, 619–628. [CrossRef]

9. Capra, L.; Manolache, M.; Ion, I.; Stoica, R.; Stinga, G.; Doncea, S.M.; Alexandrescu, E.; Somoghi, R.; Calin, M.R.; Radulescu, I. Adsorption of Sb (III) on Oxidized Exfoliated Graphite Nanoplatelets. *Nanomaterials* **2018**, *8*, 992. [CrossRef] [PubMed]

10. Russell, J.; Wilson, M. *A Hand Book of Determinative Methods in Clay Mineralogy*; Blackie and Son Ltd.: New York, NY, USA, 1987; pp. 301–320.

11. Cavallaro, G.; Lazzara, G.; Rozhina, E.; Konnova, S.; Kryuchkova, M.; Khaertdinov, N.; Fakhrullin, R. Organic-nanoclay composite materials as removal agents for environmental decontamination. *RSC Adv.* **2019**, *9*, 40553–40564. [CrossRef]

12. Jayabalakrishnan, R.; Raja, S.M. Vermiculite Clay Mineral Barrier Treatment System for Chrome Tannery Effluent. *J. Appl. Sci.* **2007**, *7*, 1547–1550.

13. Zubair, M.; Daud, M.; McKay, G.; Shehzad, F.; Al-Harthi, M.A. Recent progress in layered double hydroxides (LDH)-containing hybrids as adsorbents for water remediation. *Appl. Clay Sci.* **2017**, *143*, 279–292. [CrossRef]

14. Dos Santos, R.M.M.; Gonçalves, R.G.L.; Constantino, V.R.L.; da Costa, L.M.; da Silva, L.H.M.; Tronto, J.; Pinto, F.G. Removal of Acid Green 68: 1 from aqueous solutions by calcined and uncalcined layered double hydroxides. *Appl. Clay Sci.* **2013**, *80*, 189–195. [CrossRef]

15. Mishra, G.; Dash, B.; Pandey, S. Layered double hydroxides: A brief review from fundamentals to application as evolving biomaterials. *Appl. Clay Sci.* **2018**, *153*, 172–186. [CrossRef]

16. Moyo, L.; Focke, W.W.; Labuschagne, F.J.; Verryn, S. Layered double hydroxide intercalated with sodium dodecyl sulfate. *Mol. Cryst. Liq. Cryst.* **2012**, *555*, 51–64. [CrossRef]

17. Labuschagne, F.J.W.J.; Wiid, A.; Venter, H.; Gevers, B.; Leuteritz, A. Green synthesis of hydrotalcite from untreated magnesium oxide and aluminum hydroxide. *Green Chem. Lett. Rev.* **2018**, *11*, 18–28. [CrossRef]

18. Zhao, P.; Liu, X.; Tian, W.; Yan, D.; Sun, X.; Lei, X. Adsolubilization of 2, 4, 6-trichlorophenol from aqueous solution by surfactant intercalated ZnAl layered double hydroxides. *Chem. Eng. J.* **2015**, *279*, 597–604. [CrossRef]

19. Zaghouane-Boudiaf, H.; Boutahala, M.; Arab, L. Removal of methyl orange from aqueous solution by uncalcined and calcined MgNiAl layered double hydroxides (LDHs). *Chem. Eng. J.* **2012**, *187*, 142–149. [CrossRef]

20. Shan, R.; Yan, L.; Yang, K.; Yu, S.; Hao, Y.; Yu, H.; Du, B. Magnetic Fe3O4/MgAl-LDH composite for effective removal of three red dyes from aqueous solution. *Chem. Eng. J.* **2014**, *252*, 38–46. [CrossRef]

21. Laipan, M.; Fu, H.; Zhu, R.; Sun, L.; Steel, R.M.; Ye, S.; Zhu, J.; He, H. Calcined Mg/Al-LDH for acidic wastewater treatment: Simultaneous neutralization and contaminant removal. *Appl. Clay Sci.* **2018**, *153*, 46–53. [CrossRef]

22. Jawad, A.; Liao, Z.; Zhou, Z.; Khan, A.; Wang, T.; Ifthikar, J.; Shahzad, A.; Chen, Z.; Chen, Z. Fe-MoS4: An effective and stable LDH-based adsorbent for selective removal of heavy metals. *ACS Appl. Mater. Interfaces* **2017**, *9*, 28451–28463. [CrossRef]

23. Chen, H.; Hu, L.; Chen, M.; Yan, Y.; Wu, L. Nickel–cobalt layered double hydroxide nanosheets for high-performance supercapacitor electrode materials. *Adv. Funct. Mater.* **2014**, *24*, 934–942. [CrossRef]

24. Tabana, L.S.; Ledikwa, R.P.; Tichapondwa, S.M. Adsorption of Phenol from Wastewater Using Modified Layered Double Hydroxide Clay. *Chem. Eng. Trans.* **2019**, *76*, 1267–1272. [CrossRef]

25. Chen, Y.; Chen, H.-R.; Shi, J.-L. Construction of homogenous/heterogeneous hollow mesoporous silica nanostructures by silica-etching chemistry: Principles, synthesis, and applications. *Acc. Chem. Res.* **2014**, *47*, 125–137. [CrossRef] [PubMed]

26. Gong, M.; Li, Y.; Wang, H.; Liang, Y.; Wu, J.Z.; Zhou, J.; Wang, J.; Regier, T.; Wei, F.; Dai, H. An advanced Ni–Fe layered double hydroxide electrocatalyst for water oxidation. *J. Am. Chem. Soc.* **2013**, *135*, 8452–8455. [CrossRef] [PubMed]

27. Zhang, B.; Dong, Z.; Sun, D.; Wu, T.; Li, Y. Enhanced adsorption capacity of dyes by surfactant-modified layered double hydroxides from aqueous solution. *J. Ind. Eng. Chem.* **2017**, *49*, 208–218. [CrossRef]

28. Clariant. Available online: https://www.Clariant.com/en/solutions/products/2013/12/09/18/29/sorbacid (accessed on 14 January 2020).

29. Costa, F.R.; Leuteritz, A.; Wagenknecht, U.; Jehnichen, D.; Haeussler, L.; Heinrich, G. Intercalation of Mg–Al layered double hydroxide by anionic surfactants: Preparation and characterization. *Appl. Clay Sci.* **2008**, *38*, 153–164. [CrossRef]

30. Zhao, Y.; Li, F.; Zhang, R.; Evans, D.G.; Duan, X. Preparation of layered double-hydroxide nanomaterials with a uniform crystallite size using a new method involving separate nucleation and aging steps. *Chem. Mater.* **2002**, *14*, 4286–4291. [CrossRef]

31. Cavani, F.; Trifiro, F.; Vaccari, A. Hydrotalcite-type anionic clays: Preparation, properties and applications. *Catal. Today* **1991**, *11*, 173–301. [CrossRef]

32. Milanovic, N. *Synthesis, Structural and Magnetic Properties of Layered Double Hydroxides*; University of Oslo: Oslo, Norway, 2016.

33. Monash, P.; Pugazhenthi, G. Utilization of calcined Ni-Al layered double hydroxide (LDH) as an Adsorbent for removal of methyl orange dye from aqueous solution. *Environ. Prog. Sustain. Energy* **2014**, *33*, 154–159. [CrossRef]

34. Naseem, S.; Gevers, B.; Boldt, R.; Labuschagné, F.J.W.; Leuteritz, A. Comparison of transition metal (Fe, Co, Ni, Cu, and Zn) containing tri-metal layered double hydroxides (LDHs) prepared by urea hydrolysis. *RSC Adv.* **2019**, *9*, 3030–3040. [CrossRef]

35. Chen, L.; Li, C.; Wei, Y.; Zhou, G.; Pan, A.; Wei, W.; Huang, B. Hollow LDH nanowires as excellent adsorbents for organic dye. *J. Alloy. Compd.* **2016**, *687*, 499–505. [CrossRef]

36. Cai, W.; Yu, J.; Jaroniec, M. Template-free synthesis of hierarchical spindle-like γ-Al 2 O 3 materials and their adsorption affinity towards organic and inorganic pollutants in water. *J. Mater. Chem.* **2010**, *20*, 4587–4594. [CrossRef]

37. Hu, J.; Song, Z.; Chen, L.; Yang, H.; Li, J.; Richards, R. Adsorption properties of MgO (111) nanoplates for the dye pollutants from wastewater. *J. Chem. Eng. Data* **2010**, *55*, 3742–3748. [CrossRef]

38. Chiou, C.T. *Partition and Adsorption of Organic Contaminants in Environmental Systems*; John Wiley & Sons: Hoboken, NJ, USA, 2003.

39. Grover, A.; Mohiuddin, I.; Malik, A.K.; Aulakh, J.S.; Kim, K.-H. Zn-Al layered double hydroxides intercalated with surfactant: Synthesis and applications for efficient removal of organic dyes. *J. Clean. Prod.* **2019**, *240*, 118090. [CrossRef]

40. Gong, J.; Liu, T.; Wang, X.; Hu, X.; Zhang, L. Efficient removal of heavy metal ions from aqueous systems with the assembly of anisotropic layered double hydroxide nanocrystals@ carbon nanosphere. *Environ. Sci. Technol.* **2011**, *45*, 6181–6187. [CrossRef] [PubMed]

41. Piccin, J.; Dotto, G.; Pinto, L. Adsorption isotherms and thermochemical data of FD&C Red n 40 binding by chitosan. *Braz. J. Chem. Eng.* **2011**, *28*, 295–304. [CrossRef]

42. Dada, A.; Olalekan, A.; Olatunya, A.; Dada, O. Langmuir, Freundlich, Temkin and Dubinin–Radushkevich isotherms studies of equilibrium sorption of Zn2+ unto phosphoric acid modified rice husk. *IOSR J. Appl. Chem.* **2012**, *3*, 38–45.

43. Nethaji, S.; Sivasamy, A.; Mandal, A. Adsorption isotherms, kinetics and mechanism for the adsorption of cationic and anionic dyes onto carbonaceous particles prepared from Juglans regia shell biomass. *Int. J. Environ. Sci. Technol.* **2013**, *10*, 231–242. [CrossRef]

44. Sepehr, M.N.; Al-Musawi, T.J.; Ghahramani, E.; Kazemian, H.; Zarrabi, M. Adsorption performance of magnesium/aluminum layered double hydroxide nanoparticles for metronidazole from aqueous solution. *Arab. J. Chem.* **2017**, *10*, 611–623. [CrossRef]

45. Ayawei, N.; Ebelegi, A.N.; Wankasi, D. Modelling and interpretation of adsorption isotherms. *J. Chem.* **2017**, *2017*. [CrossRef]

46. Lupa, L.; Cocheci, L.; Pode, R.; Hulka, I. Phenol adsorption using Aliquat 336 functionalized Zn-Al layered double hydroxide. *Sep. Purif. Technol.* **2018**, *196*, 82–95. [CrossRef]

47. Chingombe, P.; Saha, B.; Wakeman, R. Sorption of atrazine on conventional and surface modified activated carbons. *J. Colloid Interface Sci.* **2006**, *302*, 408–416. [CrossRef] [PubMed]

48. Simonin, J.-P. On the comparison of pseudo-first order and pseudo-second order rate laws in the modeling of adsorption kinetics. *Chem. Eng. J.* **2016**, *300*, 254–263. [CrossRef]

49. Zhang, F.; Ni, Z.; Xia, S.; Liu, X.; Wang, Q. Removal of naphthol green B from aqueous solution by calcined layered double hydroxides: Adsorption property and mechanism studies. *Chin. J. Chem.* **2009**, *27*, 1767–1772. [CrossRef]

50. Zhu, M.-X.; Li, Y.-P.; Xie, M.; Xin, H.-Z. Sorption of an anionic dye by uncalcined and calcined layered double hydroxides: A case study. *J. Hazard. Mater.* **2005**, *120*, 163–171. [CrossRef]

51. Alcaraz, J.J.; Arena, B.J.; Gillespie, R.D.; Holmgren, J.S. Solid base catalysts for mercaptan oxidation. *Catal. Today* **1998**, *43*, 89–99. [CrossRef]